

Charge cloud asymmetry in detectors with biased MCPs

A.S. Tremsin* and O.H.W. Siegmund

Experimental Astrophysics Group
Space Sciences Laboratory
UC Berkeley
Berkeley, CA 94720

ABSTRACT

The spatial resolution of current MCP based detector devices ($<10\ \mu\text{m}$) has reached the point when such phenomenon as charge cloud asymmetry becomes important for the ultimate detector performance. We present a systematic study of the MCP charge cloud spatial distribution at the plane of the readout element. Our new readout – crossed strip (XS) anode combined with a set of preamplifiers for each anode finger – allowed us to measure directly the distribution of electrons at the anode. The measurements of the charge cloud profile were done with a high accuracy owing to the extremely high spatial resolution of the XS anode – about $5\ \mu\text{m}$ FWHM. The asymmetry of the charge cloud related to MCP channel bias was observed directly in these measurements. Our charge cloud propagation model was used to simulate the observed charge cloud asymmetry. Results of our calculations were compared with the experimental data, and a good agreement between those proves the validity of the model, which can be used for simulation of the charge cloud distribution in a wide range of detector operating parameters.

Keywords: Position sensitive detectors, Microchannel plates, spatial resolution

1. INTRODUCTION

The spatial resolution of position sensitive detectors is one of the most important parameters determining the detector efficiency for a particular application. For instance, in the area of X-ray and UV imaging, where improvement of the optical element characteristics has its own limitations, the increase of detector spatial sensitivity is the ultimate way to meet the requirements of highly demanding contemporary instrumental designs. Microchannel plate (MCP) photon counting detectors have been used quite widely in X-ray and UV imaging applications providing spatial and temporal (if required) information on every registered photon. Recently the performance of such detectors was improved substantially due to a number of advances in the readout techniques and corresponding electronics. For instance, a position resolution of $\sim 15\ \mu\text{m}$ full width at half maximum (FWHM) was achieved with crossed delay line anodes¹, of less than $10\ \mu\text{m}$ FWHM with both Vernier readout^{2,3} and subpixel centroiding in an intensified CCD⁴ and of $<7\ \mu\text{m}$ with cross strip anode⁵. At the same time the ongoing developments in the production process of glass microchannel plates should result in commercial availability of MCPs with pore dimensions as small as few microns⁶. Pore sizes smaller than a micron might potentially become widely available with the emerging manufacturing techniques such as silicon-micromachined microchannel plates^{7,8}. Consequently, the resolution of the current readout techniques and geometrical dimensions of the novel microchannel plates should allow the building of imaging photon counting detectors with a spatial resolution on the order of $5\ \mu\text{m}$. However, we have found recently that the performance of a high-accuracy detector can be degraded not only by instabilities of MCP stack operation in terms of spatial and temporal gain variation, variation of quantum detection efficiency, by noise fluctuation in the readout electronics, etc., but also by the fluctuations of the MCP charge cloud distribution if the microchannel plate has pores not perpendicular to its

* Correspondence: E-mail: ast@ssl.berkeley.edu

surface (angular-biased MCPs). Most current detectors use angular-biased MCPs (usually 5-13 degrees) to prevent the ion feedback in the detector. An alternative approach to prevent the ion feedback by utilizing curved channels was shown to be disadvantageous due to large distortions in the resulting images caused by the imperfections of the curved-channel MCPs⁹.

Previously, with spatial sensitivity of detectors on the order of $>30\ \mu\text{m}$, variation of the event position with the detector gain was not observed. It is only when the detector position sensitivity becomes lower than $\sim 30\ \mu\text{m}$ and the distance between the MCP and the readout element is relatively large ($>5\ \text{mm}$) that the spatial resolution along MCP pore bias direction may be reduced by these fluctuations of the detected photon position.

1.1. Image translational shifts due to the presence of MCP channel bias

We observed image shifts experimentally¹⁰ with a detector consisting of a Z-stack of microchannel plates and a cross delay line readout anode, which provided good linearity and a spatial resolution of about $25\ \mu\text{m}$ FWHM. The microchannel plate stack consisted of three 80:1 L/D, $12.5\ \mu\text{m}$ pores on $15\ \mu\text{m}$ centres, $36\ \text{mm}$ in diameter MCPs from Photonis-SAS. The MCP had resistances of $\sim 30\ \text{M}\Omega$, channel end spoiling of 1 pore diameter and the pore bias was 13° . A pinhole mask with $10\ \mu\text{m}$ pinholes on a $0.5\ \text{mm}$ -spaced grid with a position accuracy of $\pm 15\ \mu\text{m}$ was installed directly on the front surface of the MCP stack. A mercury vapour “pen ray” lamp ($2537\ \text{\AA}$) was used for illumination, and resolution images were accumulated at count rates of $\sim 1.5\ \text{counts}\cdot\text{sec}^{-1}$ per pinhole.

First we recorded a number of pinhole mask images obtained with different rear field voltages varying between 20 and $200\ \text{V}\cdot\text{mm}^{-1}$. An independently controlled accelerating bias of 200 - $1700\ \text{V}$ was applied in the $8.5\ \text{mm}$ gap between the MCPs and the readout anode. We observed that the entire image shifted in the direction of the MCP pore bias as the value of the accelerating electric field between the MCP output and the readout anode was varied. Fig.1 shows two superimposed pinhole mask images, taken at two different rear field voltages of 42 and $75\ \text{V}\cdot\text{mm}^{-1}$. The image displacement along the MCP pore bias axis is easily seen in the image. To verify the fact that the image shifts were caused solely by the MCP pore bias, we rotated the MCP stack by 90 degrees inside the detector, while the rest of the experimental setup was left intact. The displacements of the detector images also rotated by 90 degrees, thus confirming that the observed shifts were determined by the intrinsic properties of the MCP stack, namely the MCP pore bias. We then replaced the rear MCP in the stack with a zero degree biased microchannel plate and repeated the same measurements as with the previous detector with MCP stack in Z configuration. No displacements of the pinhole mask image were observed with the rear accelerating field varied in the range of 20 - $200\ \text{V}\cdot\text{mm}^{-1}$.

1.2. Detector walk with MCP gain

The measurements of image translational shifts discussed in the previous section indicate that the charge cloud leaving the rear MCP has a finite transverse velocity in the direction of the channel bias. Variation of the time of the cloud propagation to the anode leads to an offset of the charge cloud centroid. With fixed detector gain, accelerating rear field and distance this offset is constant for the entire active area and does not impair the detector spatial resolution. However, we found that variation of the MCP gain between individual events also leads to image shifts along the pore bias¹⁰. Therefore it is the presence of certain statistical gain variation in MCP detectors, characterized by pulse height distribution (PHD), which can consequently aggravate the instrument performance. Unlike the rear field and distance, which can be easily kept constant, the presence of PHD in each particular MCP stack can not be avoided. The presence of the charge centroid offsets with gain we call “detector walk” by analogy with electronic walk where the detector output signal is a function of gain.

To study “detector walk” phenomenon we used the same detector configuration as described in the previous section. The pinhole mask images were recorded in the form of corresponding gain and position for each registered photon. Consequently, the position of each pinhole as a function of detector gain can be extracted from that data. Fig.2 shows the walk plot images obtained in both X and Y axis (with channel pore bias directed along X-axis). One can see that the pinhole position is in direct proportion to the event gain: the larger the event gain, the larger is the pinhole displacement, while no displacements whatsoever were observed along Y-axis (perpendicular to the pore bias).

In order to verify that the observed event displacements were not an artifact induced by the readout anode or processing electronics, the microchannel plate stack was again rotated by 90 degrees within the detector. The same measurements were

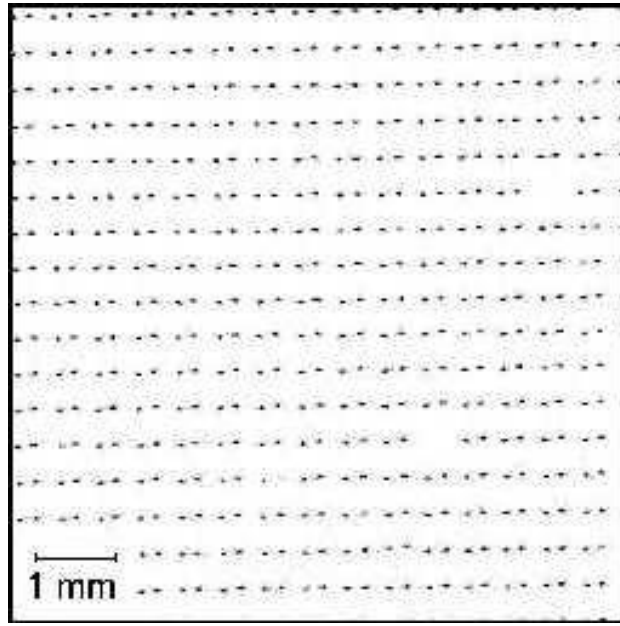


Fig.1. Two superimposed pinhole mask images obtained at 42 and 75 V/mm accelerating rear field. Detector with crossed delay line anode readout, positioned 8.5 mm below MCP (13° biased) stack operating at gain 10^7 was used in these measurements. The pinhole mask with 10 μm pinholes (500 μm apart) was installed directly on the MCP input surface. The translational shift of the entire image with rear field variation is clearly seen in this figure.

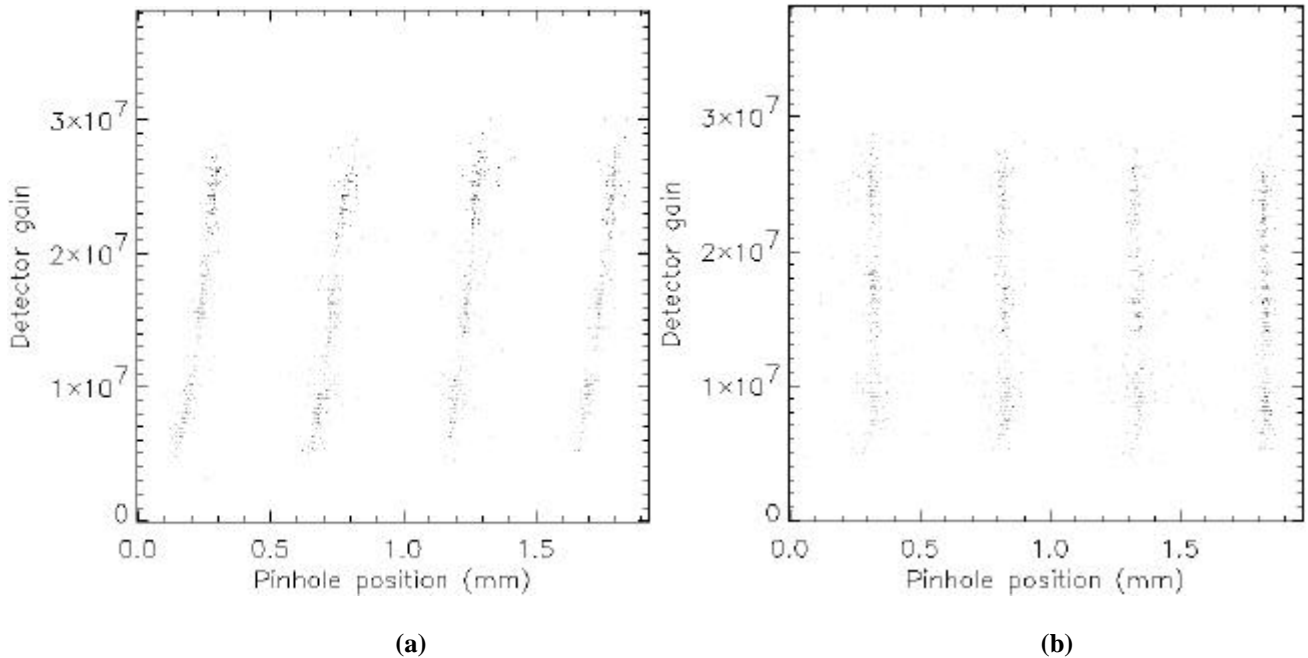


Fig.2. X-axis (a) and Y-axis (b) detector walk plots extracted from the data obtained with the same detector as in Fig.1 with a pore bias directed along x-axis. The position of each photon from 3 pinholes is plotted as a function of the event gain. The displacement of the registered photon along the direction of the pore bias is apparent in Fig2.a, while there are no displacements along Y-axis.

then repeated and we observed that the detector walk followed the direction of the rear MCP pore bias, so that X- and Y-axis walk plots merely swapped. We then again replaced MCP stack with a set of three microchannel plates, which had a zero degree biased output MCP (with front and middle plates still 13 degree-biased) and repeated the same measurements as with the previous MCP stack in Z configuration. No detector walk with gain was observed in that experiment. Both X- and Y-axes walk plots were similar to the plot presented in Fig2.b.

2. MCP CHARGE CLOUD FOOTPRINT ASYMMETRY

2.1. Previous experimental data on charge cloud asymmetry

The presence of a finite transverse velocity in the charge cloud leaving angular biased MCP obviously leads to the asymmetry of the charge footprint on the readout anode. Our colleagues at Mullard Space Sciences Laboratory have already tried to study the charge cloud footprint distribution and its asymmetry with the help of their specific charge division anode¹¹ shown in Fig.3. The split strip anode allowed them to measure simultaneously the centroid of the registered event and the proportion of charge on one side of the split (charge at electrodes A+B versus the charge at electrodes C+D). The charge distribution can then be retrieved from that information after several tens of thousands photons have been registered. They did observe some charge distribution asymmetry in their experiments, but the accuracy of their experimental data did not allow them to study the asymmetry of the charge distribution function $\tilde{\mathbf{r}}(x, y)$ in detail. Indeed, the measurement of the fractional charge $Q_{C+D}/\text{sum}Q$ resulted in the so-called ‘‘S-curve’’, which is the integral of the charge distribution projection on one of the axis. If we determine this projection along X-axis as $\mathbf{r}(x)$

$$\mathbf{r}(x) = \int_{-\infty}^{+\infty} \tilde{\mathbf{r}}(x, y) dy \cdot Q_{total}^{-1} ; \quad Q_{total} = \int_{-\infty}^{+\infty} \int_{-\infty}^{+\infty} \tilde{\mathbf{r}}(x, y) dx dy \quad (1)$$

than the ‘‘S-curve’’ measured with the split strip anode (called below $u(x)$) is an integral of $\mathbf{r}(x)$ (assuming the MCP pore bias is along the X-axis of the split strip anode):

$$u(x) = \int_{-\infty}^x \mathbf{r}(s) ds = \int_{-\infty}^{+\infty} \int_{-\infty}^x \tilde{\mathbf{r}}(s, y) ds dy \cdot Q_{total}^{-1} \quad (2)$$

The ‘‘S-curve’’ has to be differentiated in order to obtain the charge cloud distribution $\mathbf{r}(x)$ or a best-fit method of trial radial functions can be used in order to retrieve $\mathbf{r}(x)$ from the experimental data. Although the charge cloud distribution $\mathbf{r}(x)$ can be restored with a good accuracy, this data retrieval method is quite sensitive to the errors in ‘‘S-curve’’ measurements and therefore the noise in the readout electronics of the split strip anode did not allow to study the asymmetry of the charge cloud distribution $\tilde{\mathbf{r}}(x, y)$ with a high accuracy.

2.2. Calculation of the charge cloud footprint

We used our ballistic model to calculate the charge cloud distribution at the anode plane¹². This model is based on the ballistic description of the charge cloud propagation and it was modified to account for the presence of the MCP pore bias. Our model uses the differential electron distribution function at the MCP output and does not have any free parameters. The distribution function was obtained experimentally by Bronshtein et.al.¹³. The calculated projections of the charge cloud distribution $\mathbf{r}(x)$ and $\mathbf{r}'(y)$ are shown in Fig.4. The presence of the MCP pore bias in these calculations resulted in a considerable asymmetry of the charge cloud projection on the axis along the MCP channel bias. To illustrate the requirements on the accuracy of the previous split strip anode measurements, we have integrated these distributions $\mathbf{r}(x)$ and $\mathbf{r}'(y)$ according to the equation (2) and plotted them in Fig.5. There is a very small difference between these two curves despite the

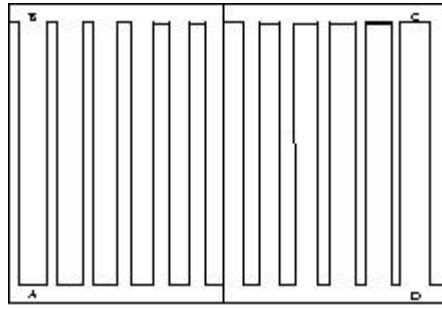


Fig.3. A schematic view of split strip anode.

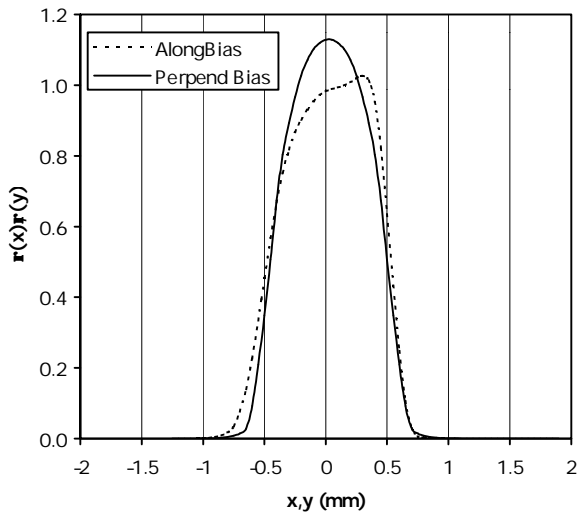


Fig.4. The two distribution functions $r(x)$ and $r'(y)$ (along MCP pore bias and perpendicular to it) calculated with the help of ballistic model at rear accelerating field of 87 V/mm and distance between the anode and the MCP 3.23 mm.

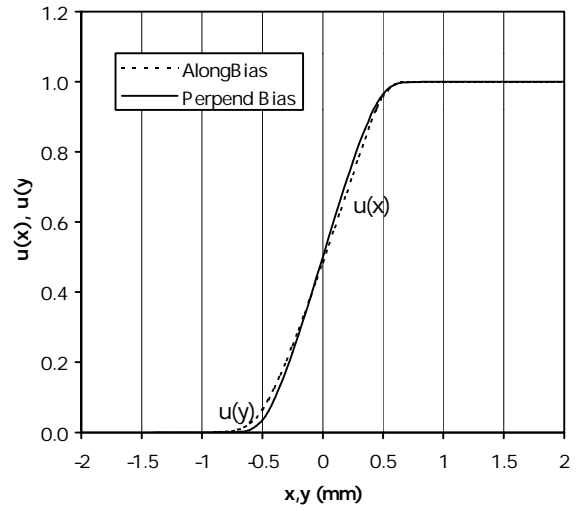


Fig.5. S-curves $u(x)$ and $u'(y)$ obtained from functions $r(x)$ and $r'(y)$ shown in Fig.4 ($r(x)$ and $r'(y)$ integrated according to equation (2)).

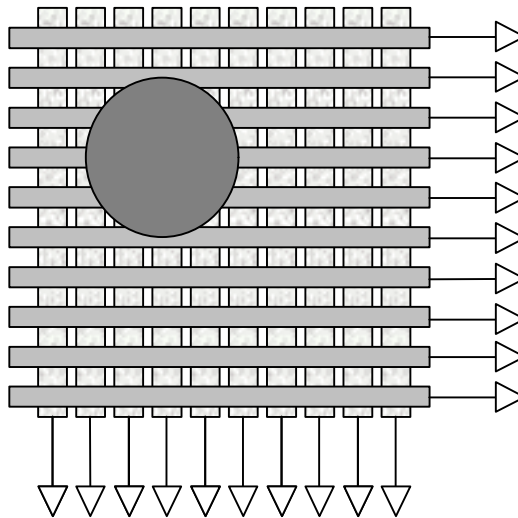


Fig.6. A schematic view of the cross strip anode.

fact that the functions $r(x)$ and $r'(y)$ are quite different. This fact demonstrates the difficulty of the charge asymmetry study with the split strip anode due to the high demands on the accuracy of this readout system.

3. MEASUREMENT TECHNIQUE

3.1. Detector and readout configuration

Our new readout, cross strip (XS) anode^{5,14}, was used in the present measurements of the charge cloud footprint. The concept of the cross strip anode is shown in Fig.6. XS anode has two orthogonal sets of conductive strips, one for X, the other for Y position encoding. The two strip sets are separate layers in a multi-layer structure and they collect the event signal from the MCP's with approximately equal charge sharing. The XS anode scheme uses the charge detected on each strip to determine the charge cloud centroid for each axis. The size of the charge cloud should be optimized so that it covers several strips in order to achieve the best spatial resolution. The anode used in the present measurements has 16 x 16 strips on a 8 mm x 8 mm format (anode period of 500 μm). The charge collected on the strips is sensed by charge sensitive amplifiers, connected individually to each strip. The preamplified signals from each strip were then digitized with two 16 channel CAMAC peak sensing 12 bit ADC's (Phillips 7164) and transferred into PC through CAMAC-PC interface manufactured by Wiener, Plein&Baus Corp. Consequently, each registered photon was represented by a set of digitized strip signal amplitudes Q_i .

A chevron stack of microchannel plates was positioned at a distance d above the XS anode and the potential V_{rear} was applied between the MCP output and the XS anode to provide an accelerating electric field. The results presented in the present paper were obtained with two different MCP stacks manufactured by Photonis SAS. Stack N1- two 80:1 L/D, 10 μm pores on 12 μm centers, 36 mm in diameter with the pore bias 13°; stack N2- two 120:1 L/D, 6 μm pores on 8 μm centers, 25 mm in diameter with the pore bias 13°.

Limited dynamic range and electronic noise of the charge amplifiers determined the range of MCP gains at which we could study the charge footprint at the anode. The feasibility of spreading the charge cloud along many fingers in order to reduce the charge injected in each amplifier and thus extending acceptable high MCP gains was limited due to the fact that the active area of our test anode was only 8x8 mm. Configuring the detector operation in the way that only few fingers have charge for each registered photon and thus lowering the low gain limit was also restrained by the fact that charge distribution can not be obtained accurately from the set of charges Q_i consisting of just few numbers.

3.2. Retrieval of the charge cloud footprint from the experimental data

In our measurements with the XS anode we obtained the set of charges Q_i from the anode fingers for each registered photon. If these charges are grouped so that all charges to the left and to the right from finger i are summed into Q_1 and Q_2 , than that data would almost exactly coincide with the data obtained with split strip¹¹ anode (with the exception that there are tiny gaps between each pair of fingers where charge is not collected). The presence of extra information on the charges to the left and to the right from finger i provides the opportunity to study the charge distribution in more details. The retrieval of the information on the spatial charge distribution at the plane of the anode in our experiments was performed in several steps. First, the position of the event centroid X_c was calculated from the set of charges Q_i :

$$X_c = \frac{\sum_i Q_i * i}{\sum_i Q_i} * P_{anode} \quad (3)$$

where P_{anode} is the anode period. The accuracy of the position centroid extraction was shown to be less than 10 μm , which is more than sufficient for our study of charge footprint at the anode as the typical dimension of the footprint is on the order of several millimeters.

The measured charge Q_i on a finger with index i is the integral of the charge distribution over the width of the finger

$$Q_i = \int_{x_i - w_f / 2}^{x_i + w_f / 2} \mathbf{r}(x) dx \quad (4)$$

where w_f is the width of XS anode fingers, used in the measurements. If width w_f is small enough, one can assume that the charge distribution function the projection of the charge distribution on the X-axis ($\mathbf{r}(x)$) does not change much within the interval $[x_i - w_f, x_i + w_f]$. Then the charge distribution $\mathbf{r}(x)$ can be approximated to be constant within that interval:

$$\mathbf{r}^*(x_i) = \frac{Q_i}{w_f \sum_i Q_i} \quad (5)$$

where x_i is the center of the finger with index i ($x_i = P_{anode} * i$). Therefore for each registered photon we can find the value of the charge distribution function $\mathbf{r}(x)$ in several points x_i . Now, for each event we shift axis X so that the center of the charge distribution is always in the center:

$$x_i^* = x_i - X_c \quad (6)$$

As a result, for each event we know the charge distribution function $\mathbf{r}(x^*)$ in several points x_i^* . Collecting a large number of events with flat field illumination of the detector provides information on the charge distribution $\mathbf{r}(x^*)$ for all x^* coordinates, since X_c under the flat field illumination is changing continuously within the active area.

The described method of charge distribution retrieval from the experimental data obtained with a XS anode still requires certain assumptions to be made. First, we can study only the averaged spatial distribution of the MCP charge cloud over several thousands of events. Therefore in the current study, similar to the previous investigation¹¹, we have to use an assumption that the distribution does not change from one event to another and also within the MCP active area. In addition to that, our method is still not a completely explicit way of measuring the charge distribution due to the presence of a finite width of the anode fingers (the assumption of equation (5) on the small width w_f of the fingers in the anode).

4. EXPERIMENTAL RESULTS

4.1. Variation of MCP charge footprint with rear accelerating field

First we investigated variation of the charge cloud footprint with the rear accelerating field V_{rear} . The MCP chevron stack N1 was positioned at a distance of 5.45 mm above the XS anode and a constant bias of 2100V was applied across the MCPs, while the rear field voltage was independently controlled within the range of 23 and 111 V/mm. Fig.7 summarizes the results of these measurements. The projections of the charge distribution on the axis perpendicular to the channel pore bias are plotted as a function of distance from the charge distribution center. The gain of the MCP stack during these measurements was about 10^6 . We did not observe any large changes in the shape of the charge cloud distribution except for the obvious decrease of the footprint radius from 3mm to 1.5mm while the rear field changed from 23 and 111 V/mm.

4.2. Variation of charge footprint with MCP gain

We continued with measurements of the charge distribution at a fixed value of rear accelerating field of 87 V/mm. The MCP stack bias was changed between 2000V and 2215V, corresponding to MCP gain variation between 7×10^5 and 3×10^6 . The corresponding pulse height distributions of the detector are shown in Fig.8. Both charge distributions (along the MCP pore bias and perpendicular to it) were measured in these experiments. First the MCPs were positioned in the detector with the pore bias along X-axis and charge distributions were measured. Then the MCP stack was rotated by 90 degrees in the

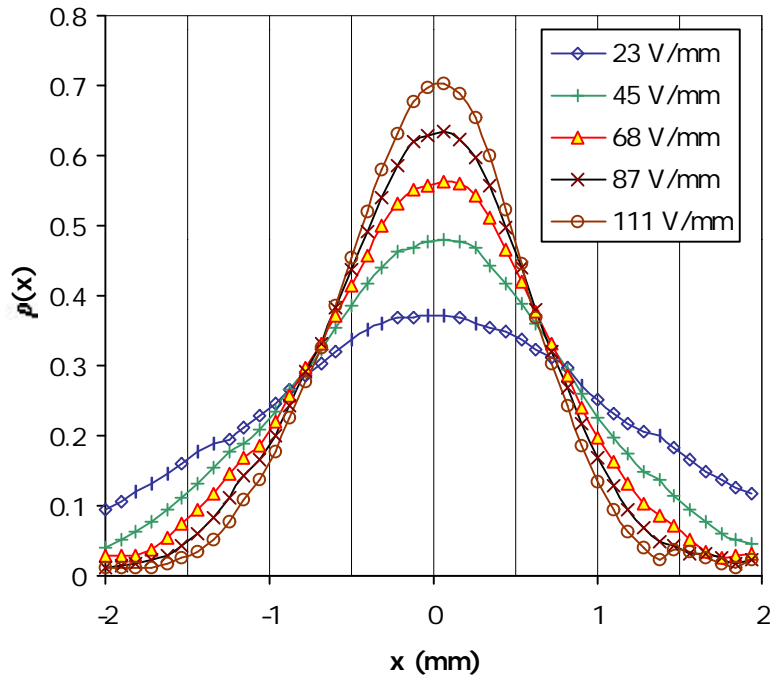


Fig.7. Measured variation of the charge cloud footprint with the rear accelerating field. MCP pore bias is perpendicular to X-axis. The anode-to-MCP distance is 5.45 mm with the rear field voltage values shown in the legend. MCP gain 10^6 .

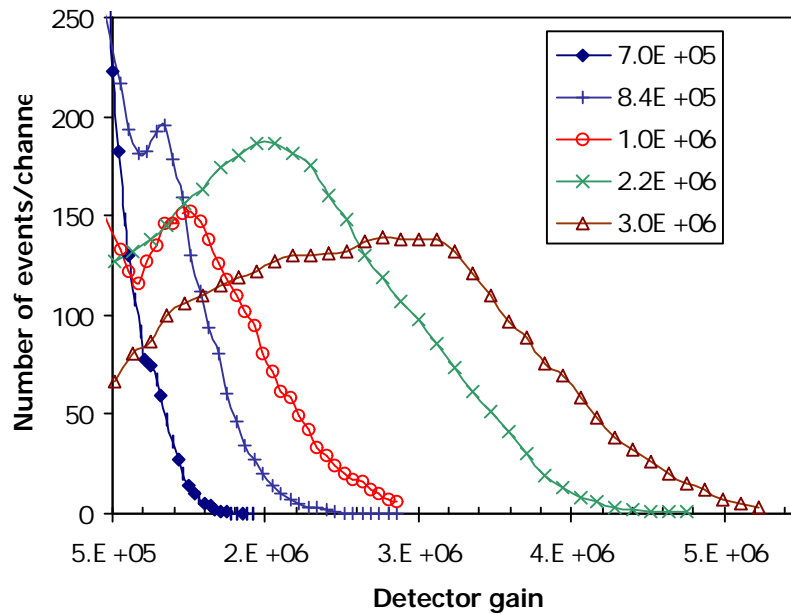


Fig.8. Pulse height distributions of the MCP stack used in measurements of the charge footprint variation with MCP gain.

detector so that the same set of fingers was used to study the charge footprint at two different MCP orientations. Thus we avoided any data inconsistency due to the differences of the finger width of the top and bottom electrodes on the XS anode. Fig.9.a and Fig.9.b show the results of these measurements. We did observe apparent footprint asymmetry with the charge distribution shifted along the pore bias (see Section 4.3 for more details).

4.3. Asymmetry of MCP charge distribution

To study the charge distribution asymmetry we measured the charge footprint with MCP stack N2 positioned in the detector so that the pore bias coincided with the X-axis and with the pore bias in the opposite direction. This was achieved by rotating the MCP stack in the detector by 180 degrees after the first set of measurements. The distance to the anode in these experiments was 3.23 mm. The MCP bias was 2700V resulting in the detector gain of $\sim 10^6$ and the rear accelerating field of 87 V/mm was applied between the MCP output and the anode. Fig.10.a shows the measured charge distributions for both MCP orientations in the detector. Asymmetry of the charge cloud footprint at the anode is clearly seen in that image. To verify that the asymmetry is determined only by the MCP pore bias and not by any inaccuracies of the readout and its processing electronics, we plotted the same data as in Fig.10.a but with one distribution rotated along the Y-axis (flipped horizontally), Fig.10.b. The two curves almost exactly match each other proving that only the signal from MCP stack induces the shift of the charge distribution along the pore bias.

The experimentally obtained charge distribution along the pore bias, presented in Fig.10.a and the distribution calculated for the detector with the same parameters (Fig.4) seem to be in a good agreement. However, our ballistic model does not allow us to calculate variation of the charge footprint with MCP gain since the experimentally measured distribution function at the MCP output¹² was obtained only at a particular MCP gain, although the model itself is not limited to fixed MCP gain operation.

5. CONCLUSIONS

The present study of the MCP charge cloud distribution at the plane of the anode demonstrates how the novel cross strip anode can be used to measure the projections of the charge footprint at two orthogonal axes. The results of these measurements prove the presence of the asymmetry along the MCP pore bias. It indicates that in high accuracy detectors utilizing angular biased microchannel plates for electron multiplication the detector configuration and parameters of its operation should be optimized in order to eliminate the “detector walk” phenomena¹⁰, which can substantially decrease the spatial resolution of the device in the direction of the pore bias. We have measured directly the increase of the charge footprint radius with the increase of MCP gain. The radius of the charge distribution was also measured to increase from ~ 1.5 mm to ~ 2 mm when the rear field voltage was reduced from 111 to 23 V/mm.

In order to reduce the influence of the observed charge distribution variations on ultimate detector performance the MCP pore bias should always be aligned along one of the axes of the instrument, which has less demanding requirements on the spatial resolution (e.g. in spectroscopical devices, as it was used in FUSE detector¹, for example). At the same time reducing the distance between the MCP stack and the readout anode can also reduce the influence of the footprint variation on the detector spatial resolution. It is worth emphasizing here that the cross strip readout does allow positioning MCP stack at a very small distance from the anode.. The ability of this readout to achieve spatial resolution of several microns FWHM may be partially explained by the short distance to the anode in the measurements reported in ref⁵.

In the present study we did not address the question of how different is the charge distribution in detectors with different MCPs and the same MCPs operating at different conditions. For instance, the investigation of the influence of electrode endspoiling on the spatial properties of the MCP output signal, and the role of MCP saturation stage, as well as measurements with MCP possessing different pore inclinations are in our future experimental plans.

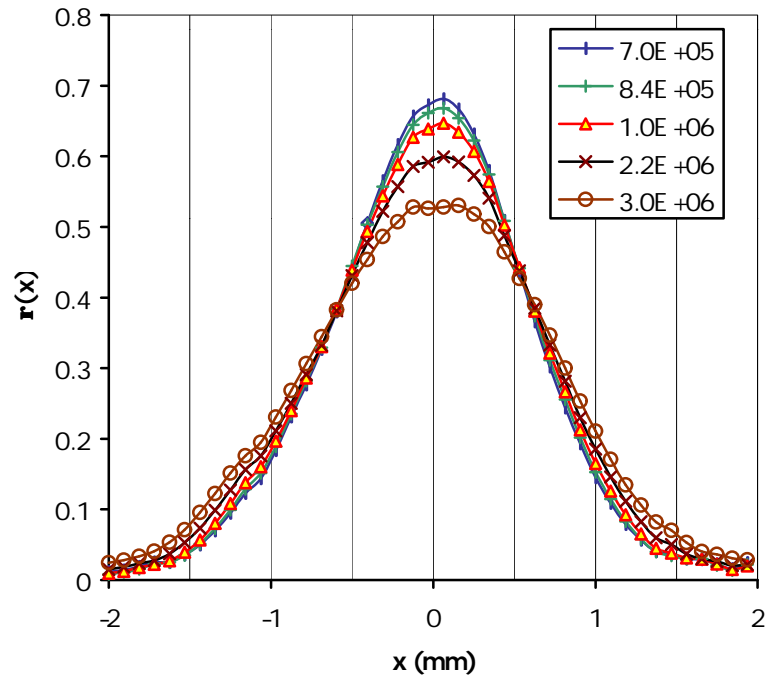


Fig.9.a. Measured variation of the charge cloud footprint with MCP gain. Charge distributions are measured along the axis, which was perpendicular to the MCP pore bias. The corresponding gains are shown in the legend. The rear accelerating field fixed at 87 V/mm in 5.45 mm MCP-anode gap.

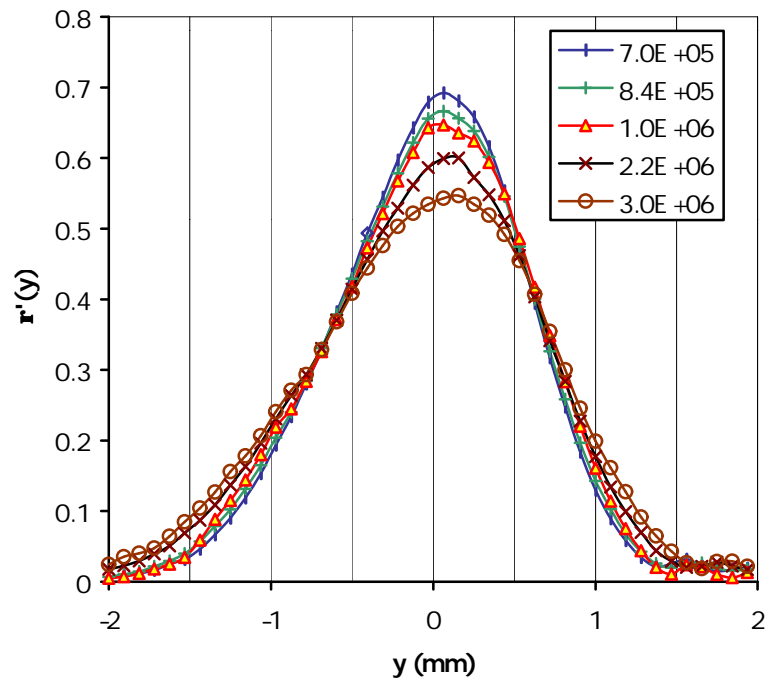


Fig.9.b. Measured variation of the charge cloud footprint with MCP gain. Charge distributions are measured along the axis coinciding with the MCP pore bias. The corresponding gains are shown in the legend. The rear accelerating field fixed at 87 V/mm in 5.45 mm MCP-anode gap.

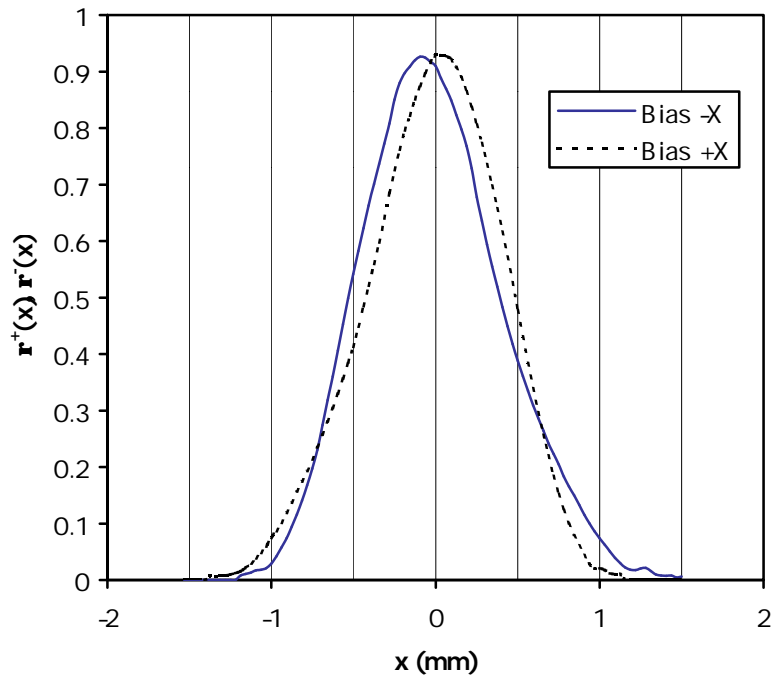


Fig.10.a. Charge distribution functions at the plane of the anode obtained with MCP pore bias aligned along X-axis and MCPs pore bias aligned opposite to X-axis (MCP was rotated by 180 degrees). The rear accelerating field fixed at 87 V/mm in 3.23 mm MCP-anode gap. Detector gain $\sim 10^6$. The asymmetry of the charge distribution is clearly seen.

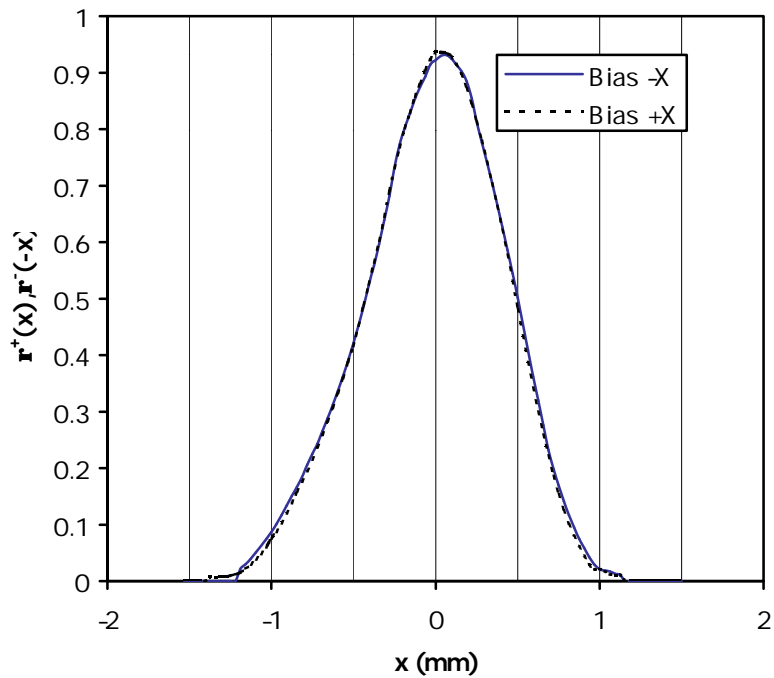


Fig.10.b. The same data as in Fig.10.a, but with one of the curves flipped horizontally. Two distributions obtained at opposite MCP pore bias match each other.

6. ACKNOWLEDGEMENTS

This work was supported by NASA grant NAG5-8667. The authors would like to thank Dr. J. Millaud, Dr. P. F. Manfredi and Dr. V.V. Souchkov from Lawrence Berkeley National Laboratory for their help with the readout electronics and George Zizka for his help with front-end chip wirebonding.

7. REFERENCES

1. O. H. W. Siegmund, M. A. Gummin, J. M. Stock, G. Naletto, G. A. Gaines, R. Raffanti, J. Hull, R. Abiad, T. Rodriguez-Bell, T. Magoncelli, P. Jelinsky, W. Donakowski, K.E. Kromer, "Performance of the double delay line microchannel plate detectors for the Far-Ultraviolet Spectroscopic Explorer", in *X-Ray, and Gamma-Ray Instrumentation for Astronomy VIII*, O. H.W. Siegmund; M. A. Gummin; Eds. Proc. SPIE **3114** pp. 283-294 (1997).
2. J. S. Lapington, B. S. Sanderson, L. B. Worth, "The Vernier electronic readout: high resolution and image stability from a charge division readout for microchannel plates", in *X-Ray, and Gamma-Ray Instrumentation for Astronomy IX*, O. H.W. Siegmund; M. A. Gummin; Eds. Proc. SPIE **3445**, pp. 535-545 (1998).
3. J. S. Lapington, B. Sanderson, L. B. C. Worth, "Imaging achievements with the Vernier readout", Proc. 5th International Conference on Position-Sensitive Detectors, University College London 13-17 September 1999 (to be published in Nucl. Instr. and Meth. A).
4. J. V. Vallerga, O. H. W. Siegmund, J. Dalcomo, P. N. Jelinsky, "High-resolution (<10-um) photon-counting intensified CCD", in *Solid State Sensor Arrays: Development and Applications*, Morley M. Blouke; Ed., Proc. SPIE **3019**, pp.156-167 (1997).
5. O. H. W. Siegmund, A. S. Tremsin, J. V. Vallerga and J. Hull, "Cross strip anode imaging readouts for microchannel plate detectors", IEEE Nuclear Science Symposium and Medical Imaging Conference, October 15-20, 2000, Lyon, France. To appear in IEEE Trans. Nucl. Sci.
6. B. N. Laprade, R. C. Cochran, F. Langevin, M. W. Dykstra, "Characterization of an ultrasmall-pore microchannel plate" in *Ultrahigh- and High-Speed Photography and Image-based Motion Measurement*, D. R. Snyder; A. Davidhazy; T. Etoh; C. B. Johnson, J. S. Walton; Eds., Proc. SPIE **3173**, pp. 474-485 (1997)
7. C. P. Beetz, R. B. Boerstler, J. Steinbeck, B. Lemieux, D. R. Winn, "Silicon-Micromachined Microchannel Plates", Nucl. Instrum. Methods A **442**, pp. 443-451 (2000).
8. O. H. W. Siegmund, A. S. Tremsin, J. V. Vallerga, C. P. Beetz, Jr., D. R. Winn, "Silicon microchannel plates: initial results for photon counting detectors", in *X-Ray and Gamma-Ray Instrumentation for Astronomy X*, Proc. SPIE **4140** pp.188-198 (2000).
9. S. N. Osterman, G. J. Rottman, D. M. Hassler, et al., "Comparison of the imaging characteristics of curved-channel and straight-channel microchannel plates", Applied Optics **36**, pp. 753-759 (1997).
10. A. S. Tremsin, J. V. Vallerga, O. H. W. Siegmund, "Detector walk" in position-sensitive detectors with biased microchannel plates", Review of Scientific Instruments **71**, pp.3758-3761 (2000).
11. M. L. Edgar, R. Kessel, J. S. Lapington, D. M. Walton, "Spatial charge cloud distribution of microchannel plates", Rev. Sci. Instrum. **60**, pp.3673-3680 (1989)
12. A. S. Tremsin, O. H. W. Siegmund, "Spatial distribution of electron cloud footprints from microchannel plates: measurements and modelling", Review of Scientific Instruments **70**, pp.3282-3288 (1999).
13. I. M. Bronshteyn, A. V. Yevdokimov, V. M. Stozharov, A. M. Tyutikov, Radio Engng. Electron. Phys. **24**, p.150 (1979).
14. O. H. W. Siegmund, J. S. Hull, A. S. Tremsin, J. Zaninovich, "Cross-strip anodes for microchannel plate imaging detectors", in *EUV, X-Ray, and Gamma-Ray Instrumentation for Astronomy IX*, Proc. SPIE **3445**, pp.397-406 (1998).